

Microstructural Characterization and Self-Propagation Properties of Reactive Al/Ni Multilayers Deposited onto Wavelike Surface Morphologies: Influence on the Propagation Front Velocity

Yesenia H. Sauni Camposano,* Heike Bartsch, Sebastian Matthes, Manuel Oliva-Ramirez, Konrad Jaekel, and Peter Schaaf

Reactive multilayer systems are nanostructures of great interest for various technological applications because of their high energy release rate during the self-propagating reaction of their components. Therefore, many efforts are aimed at controlling the propagation velocity of these reactions. Herein, reactive multilayer systems of Al/Ni in the shape of free-standing foils with a wavelike surface morphology prepared by using sacrificial substrates with well-aligned waves are presented and the propagation of the reaction along different directions of the reproduced waves is analyzed. During the ignition test, the propagation front is recorded with a high-speed camera, and the maximum temperature is measured using a pyrometer. The propagation of the reaction is favored in the direction of the waves, which points out the influence of the anisotropy generated by this morphology and how it affects the propagation dynamics and the resulting microstructure. Furthermore, compared to their counterparts fabricated on flat substrates, these reactive multilayers with wavelike morphology exhibit a remarkable reduction in the propagation velocity of the reaction of about 50%, without significantly affecting the maximum temperature registered during the reaction.

1. Introduction


Reactive multilayer systems (RMS) consist of two or more reactive components in the shape of nanolayers that are alternately stacked on top of each other following a systematic periodicity. These components react exothermically if the RMS is heated up locally, triggering both the atomic diffusion that occurs normal to the layers and the thermal diffusion of released heat that occurs parallel to the layers. Consequently, the reaction extends to the unreacted areas, establishing a self-sustained propagating heat wave until all reactants are consumed.^[1,2] In the reaction process of the binary system of Al/Ni (RMS Al/Ni), the energy released, well known as the heat of reaction, and the velocity of propagation are features of great interest for diverse technological applications. Including their use in bonding,^[3] thermal batteries,^[4] and the synthesis of high entropy alloys.^[5]

Y. H. Sauni Camposano, S. Matthes, M. Oliva-Ramirez, P. Schaaf
Chair Materials for Electrical Engineering and Electronics
Institute of Materials Science and Engineering
Institute of Micro and Nanotechnologies MacroNano
TU Ilmenau
Gustav-Kirchhoff-Str. 5, 98693 Ilmenau, Germany
E-mail: yesenia.sauni@tu-ilmenau.de

H. Bartsch, K. Jaekel
Electronics Technology Group
Institute of Materials Science and Engineering
Institute of Micro and Nanotechnology MacroNano
TU Ilmenau
Gustav-Kirchhoff-Str. 1, 98693 Ilmenau, Germany

M. Oliva-Ramirez
Nanotechnology on Surfaces and Plasma Laboratory
Instituto de Ciencia de Materiales de Sevilla
CSIC-Universidad de Sevilla
Avda. Américo Vespucio 49, 41092 Sevilla, Spain

M. Oliva-Ramirez
Departamento de Física Atómica
Molecular y Nuclear
Universidad de Sevilla
Avda. Reina Mercedes, 41012 Sevilla, Spain

 The ORCID identification number(s) for the author(s) of this article can be found under <https://doi.org/10.1002/pssa.202200765>.

© 2023 The Authors. physica status solidi (a) applications and materials science published by Wiley-VCH GmbH. This is an open access article under the terms of the Creative Commons Attribution License, which permits use, distribution and reproduction in any medium, provided the original work is properly cited.

DOI: 10.1002/pssa.202200765

Therefore, theoretical and experimental investigations have been carried out to elucidate the dependence of the reaction characteristics on parameters such as the atomic composition ratio, the bilayer thickness, and the premixed thickness at the interface of RMS.^[6–11] It was demonstrated that the velocity of the reaction depends inversely on the thickness of the bilayer simply because of the increase of the diffusion distance in thicker bilayers. However, below a critical bilayer period, the reaction rate and the propagation velocity are strongly affected by the premixed interfaces between the layers.^[6,12,13] This is because the amount of stored chemical energy in RMS can be reduced due to the chemical intermixing of reactants prior ignition, resulting in a reduction in the velocity of the reaction.^[6,12] The influence of the substrate surface on the RMS structure and phase transformation was recently explored, showing the impact of the substrate roughness on the premixed thickness of the as-deposited RMS and on the phase transformation during annealing.^[14,15] However, the dynamics of the reaction promoted by slow heating rates, such as annealing or differential scanning calorimetry (DSC), differs from a self-propagating reaction, where the formation of the AlNi intermetallic phase occurs directly from a liquid–solid state, whereas during annealing the diffusion of the reactants occurs in the solid state.^[16] Schultz et al. recently showed the influence of the substrate topography on the propagation velocity by depositing RMS on low-temperature co-fired ceramic (LTCC) with previous surface modification.^[17] The rough surface of the substrate affected the propagation velocity and improved the adhesion between the substrate and the multilayers after ignition. These effects can be interesting for bonding applications where slow propagation fronts are needed. However, deeper investigations are necessary to understand the impact of the surface topography on the microstructure of the RMS and on the propagation behavior of the reaction. In addition, many efforts to control the reaction velocity in RMS were reported. Fritz et al. fabricated low-density compacts by funneling multilayer particles into a glass tube, thus achieving low propagation velocities.^[18] Danzi et al. show the possibility of reducing and increasing the propagation velocity by adding alloying elements in the multilayers.^[19] Therefore, in this study we focus on the effect of the substrate surface

topography, on the morphology of the produced Al/Ni reactive multilayers with wavelike surface morphology (W-RMS), and on its consequent influence in the self-propagating reaction. In contrast to previous research, where the substrate presented structures in the order of micrometers and an isotropic surface texture,^[17] in this work the surface of the copper substrate presents fine ridges or waves with a preferred orientation, which, despite their nanometric size, affects the growth of the Al/Ni layers and the propagation dynamics of the reaction. Besides, rolled copper foils are used as substrates because it is a competitive alternative to 2D fabrication methods, which are usually expensive and resource-intensive. The surface topography and surface roughness of the as-deposited multilayers were investigated using scanning electron microscopy (SEM) and atomic force microscopy (AFM). The propagation velocity of the reaction front was recorded using a high-speed camera and the maximum temperature by a high-speed pyrometer. The composition of the layers before and after the reaction was determined by X-ray diffraction (XRD) analysis.

2. Experimental Section

2.1. Sample Preparation

In order to obtain RMS with wavelike surface morphologies (W-RMS), Al/Ni multilayers were deposited onto commercially rolled copper foil of 99.9% of purity and 127 μm of thickness (Alfa Aesar). **Figure 1** shows the wavy surface produced by their rolling fabrication process. To elucidate the influence of the wavy substrate compared to a flat substrate, analogous Al/Ni multilayers were also deposited on Si (100) wafers (Siegert wafer) presenting a flat surface which will be used as a reference sample. The Al and Ni layers were deposited by direct current (DC) magnetron sputtering in a cluster deposition system (CS400 by Von Ardenne). The process was carried out at room temperature and at a working pressure of 5×10^{-3} mbar, and the sputtering power and the argon flow were set at 200 W and 30 sccm, respectively. The distance between the substrate and the targets of Al (99.99% purity, FHR) and Ni (99.99% purity, FHR) was set at 105 mm, resulting in a deposition rate of 0.32 nm s^{-1} for

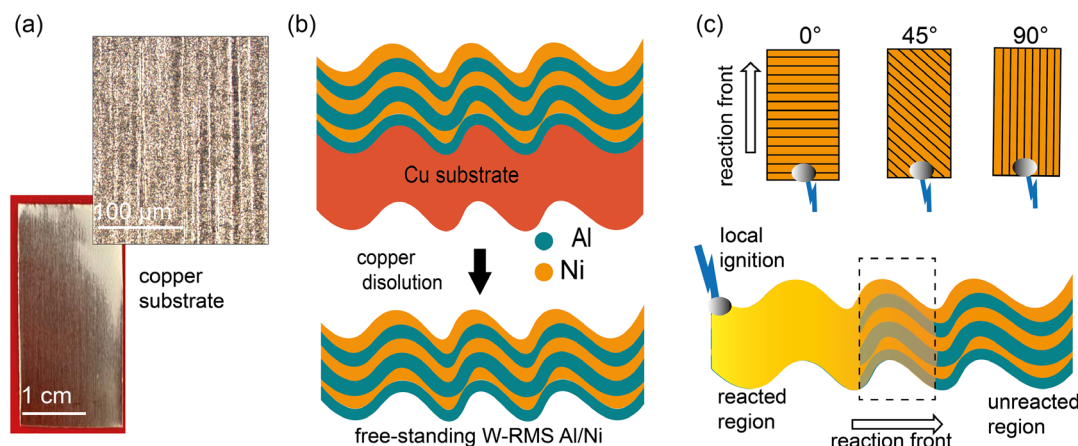


Figure 1. a) Picture of the copper foil (substrate) and inset of surface view under light microscopy; b) scheme of the fabrication flow of the freestanding W-RMS; c) illustration of ignition process and cross-sectional schematic of a self-propagating reaction along the W-RMS.

aluminum and 0.26 nm s^{-1} for nickel. The total thickness of the RMS is $5 \mu\text{m}$ with a bilayer periodicity of 100 nm ; the individual thicknesses of the Al and Ni layers were adjusted to obtain a 2:3 atomic ratio. Subsequently, the copper substrate was removed using a solution of ammonium peroxydisulfate ($C = 1.3 \text{ mol L}^{-1}$). After the dissolution of the copper, the samples were washed in baths of acetone, isopropanol, and water. Samples 30 mm long and 15 mm wide were prepared with the waves oriented parallel (90°), perpendicular (0°), or diagonal (45°) to the longest side of the sample, as shown in Figure 1. For simplicity, we will refer to the fabricated foils as 0° , 45° , and 90° . On the other hand, the flat multilayers were mechanically peeled from the Si substrate. The chemical reaction of the obtained free-standing W-RMS was activated by an electric spark in air and at room temperature.

2.2. Analysis Methods

To investigate the microstructural features of the W-RMS Al/Ni deposited on copper substrates, cross sections of the multilayers were prepared by focused ion beam (FIB) nanomilling (Auriga 60, Zeiss) and cross-sectional views were recorded with the integrated SEM. Top-view micrographs of the surface before and after ignition were obtained using SEM (S-4800 HITACHI). In both cases, the operating voltage was set at 5 kV . In order to determine the chemical composition of the foils after the reaction, energy-dispersive X-ray spectroscopy (EDX) was performed with an operating voltage of 25 kV . The roughness and topography of the as-deposited RMS were studied using an atomic force microscopy (AFM) (Dimension Veeco), with a scan rate of 0.30 Hz and an amplitude of 294.3 mV for a scan size of $50 \mu\text{m}$. AFM images were processed with the WSxM 5.0 software.^[20] During the ignition test, the propagation of the reaction was recorded by a high-speed camera (FASTCAM SA-X2 type 480 K) with a resolution of $50\,000 \text{ fps}$, and the net velocity of the propagation was measured by using Image J software with manual tracking.^[21] The surface temperature of the ignited sample was measured by a high-speed pyrometer (KLEIBER-Pyrometer Pyroskop 840) with an emissions coefficient value (ϵ) fixed to 1 and a resolution time of $10 \mu\text{s}$. XRD analysis was performed before and after ignition using the Bruker D5000 Theta-Theta X-ray diffractometer, equipped with a $\text{Cu K}\alpha$ ($\lambda = 0.15418 \text{ nm}$) radiation source used at 40 kV and 40 mA , working in Bragg–Brentano mode with a scan speed of 1 s per step and a 2θ increment of 0.02° . The obtained diffraction patterns were analyzed in the 2θ range of $30\text{--}100^\circ$ by using Bruker Diffrac. EVA software tool.^[22]

3. Results

3.1. Characterization of the Surface Topography

The surface topography of the rolled copper presents waves that are produced during the rolling process due to the elongation of the copper grains. During the deposition process, the surface topography of the copper substrates was reproduced on the deposited Al/Ni multilayers. The transferred structure can be seen with the naked eye and their orientation can be clearly

distinguished. A closer view of the surface of the W-RMS Al/Ni in Figure 2 shows clearly the reproduced waves and their well-aligned orientation. However, as the surface of the substrate shown in Figure 1, the distribution of the waves in the surface of the W-RMS is a bit ragged and presents disruptions and defects. In fact, in some areas the defects are large enough to disturb the order and orientation of the waves as observed in the insets of Figure 2b. The waves on the W-RMS offer a structure with elongated patterns as shown in Figure 2d, where the distribution of these patterns can be observed. The patterns vary in width and length, most have an elongated shape and are oriented in the same direction; however, domains with different shapes can be observed in some areas. Therefore, a texture analysis was performed to evaluate the surface.

The surface texture was evaluated using the frequency analysis tool in Mountains Map software, which uses an algorithm based on the Fourier transform modulus of the image to calculate the orientation angle of the texture and the degree of isotropy.^[23] An isotropy value of 100% of means that the texture is completely isotropic and there is no main texture orientation; on the other hand, 0% means that the texture is strongly oriented, and thus it is considered as an anisotropic texture. The texture direction analysis was performed using the obtained SEM micrographs, and the results are depicted in a polar graph as shown in Figure 2c, where the obtained isotropy is 2.4% and the preferential orientations are 90° and 95° , first and second direction, respectively. This analysis was performed in different areas of the sample surface and the isotropy varies from 1.8% to 3.6%. Consequently, we can conclude that the produced W-RMSs have a strongly oriented texture that was transferred from the substrate to the Al and Ni layers.

In order to evaluate the surface roughness, AFM analyses were performed for the W-RMS and for the reference sample deposited on flat Si wafers. As it can be seen in Figure 3, the difference in roughness is evident. The roughness (R_z) calculated for the multilayers deposited on copper foils varies from 120 to 160 nm , whereas the R_z calculated for the multilayers on Si is in the range between 7 and 11 nm . Additionally, the topographic and 3D images reveal deep clefts in the surface of the W-RMS, which are not aligned with the waves.

Figure 4a shows a cross-sectional view of the as-deposited W-RMS and it exhibits how the topography of the substrate is reproduced in the multilayers of Al and Ni. Unlike the multilayers that were deposited on flat silicon, the multilayers deposited on Cu show multiple defects in the surface and present high surface roughness with a strongly oriented texture. In addition, they show surface and bulk defects caused by the growth on the patterned copper substrate. Note in Figure 4b1 how the deep valley of the surface of the substrate causes a bulk defect, well known as hole-like defects, in the W-RMS.^[24]

3.2. Self-Propagating Reaction

3.2.1. Net Velocity and Maximum Temperature

The reaction of the free-standing Al/Ni W-RMS (0° , 45° , and 90°) and the reference sample was initiated by spark ignition. The analysis of the propagation front of the flame was initially carried out by calculating the net velocity of propagation, which was

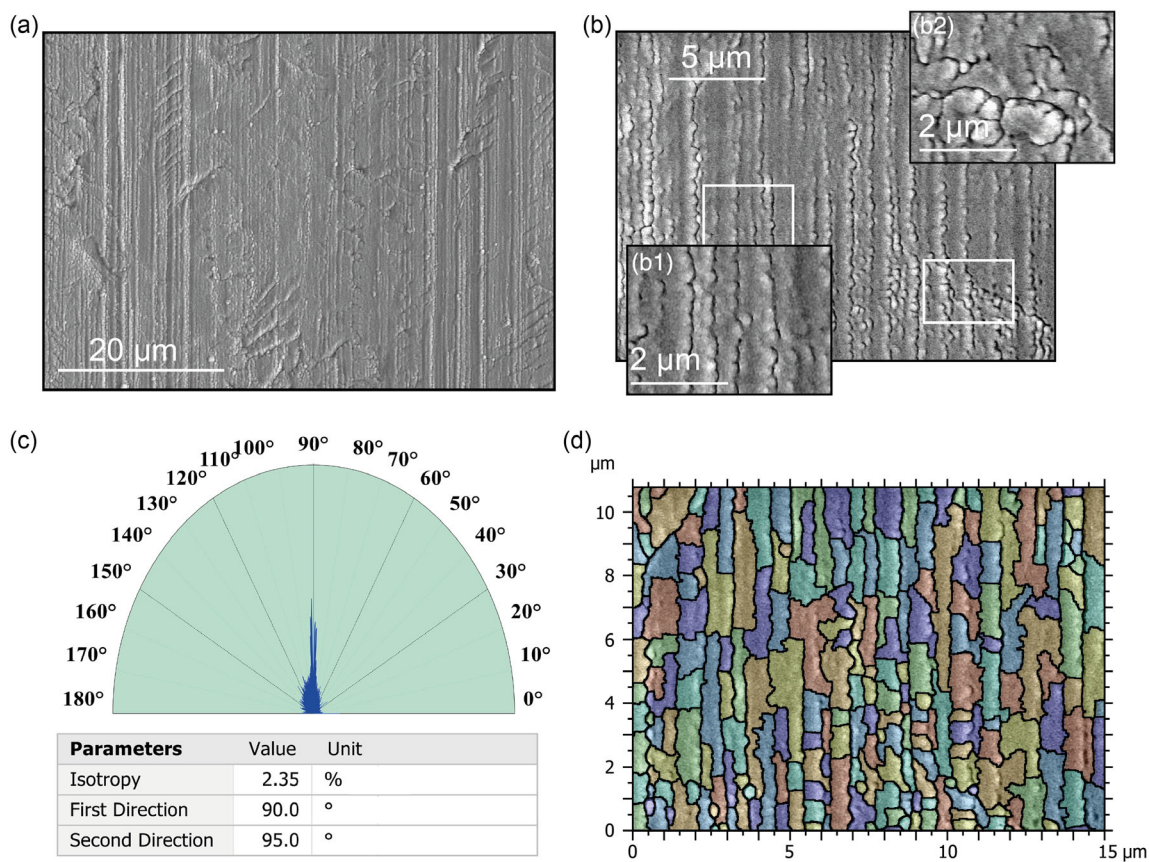


Figure 2. a,b) SEM images of the Ni/Al multilayers deposited on the Cu substrate after dissolution of the substrate; c) analysis of the texture direction obtained from (a), using frequency analysis in MountainsMap software; d) distribution of the elongated patterns analyzed by the watershed filter in MountainsMap software.^[23]

measured in the same direction for all the samples independently of the wave's orientation. As shown in **Figure 5a**, the net velocity was measured in the direction parallel to the longest side of the sample, starting at the ignition point until the sample is consumed. During the ignition test, the maximum temperature of the flame (T_{\max}) was also registered by using a pyrometer. The obtained results are listed in **Table 1**; the mean value and the standard deviation (SD) for each different configuration of the samples were also calculated.

Figure 5a shows sequential images of the propagation front obtained during the reaction of the multilayers, where the difference between the propagation front generated in the systems with wavy morphology and the reference sample can be observed. The values of net velocity and the maximum temperature registered during the ignition test are plotted in Figure 5b.

The net velocity obtained from the W-RMS varies drastically for each sample from 1.2 to 2.1 m s^{-1} , unlike the reference sample, which shows a stable velocity about $2.4 \pm 0.05 \text{ m s}^{-1}$. In addition, the maximum temperature registered for each sample is also visible in Figure 5a, the reference samples reach temperatures from 1350 to 1412 K, and the maximum temperature of the W-RMS varies from 1243 to 1330 K. Due to the variation in the results, no trend related to the configuration of the waves direction can be established at this point. However, it is evident

that the temperature and velocity decrease for the W-RMS in comparison with the reference samples. It is well known that the change in the temperature will exponentially impact the kinetics of the reaction; thus, in several analytical models the velocity of propagation is directly related to the temperature of the flame.^[1,2,25] Grapes et al. derived Armstrong's analytical model to obtain the Arrhenius function for laminar materials which relates the velocity of propagation and the temperature of the flame (see Equation (1))^[7,25]

$$\frac{\ln(V_x^2(T_{\max} - T_0)/B * T_{\max}^2)}{d(1/T_{\max})} = -\frac{E_a}{R} \quad (1)$$

Where V_x is the propagation velocity, R the gas constant, T_{\max} the maximum temperature, E_a the activation energy, T_0 the initial temperature, and B is a reference value with units $\text{K s}^{-2} \text{ m}^{-2}$. In order to obtain the Arrhenius plot shown in **Figure 6**, experimental data from Table 1 were replaced into Equation (1), where T_0 is the room temperature (298 K) and B is $1 \text{ K s}^{-2} \text{ m}^{-2}$.

The results show an evident negative slope characteristic of reactive materials and it can be approximated to a straight line; as a result, the calculated activation energy is 91.2 kJ mol^{-1} . As expected the data are considerable scatter and at least 3 points are not close to the linear fit; therefore, a deeper analysis is necessary.

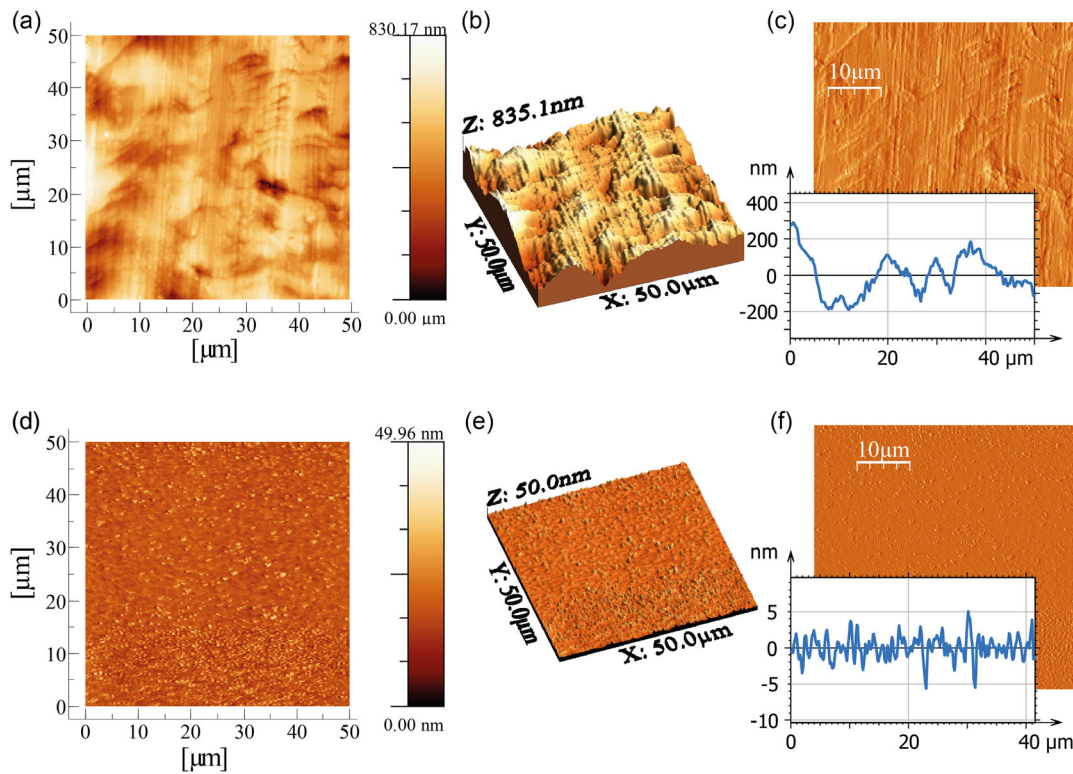


Figure 3. a) Topographic, b) 3D, and c) amplitude; AFM images of the as-deposited W-RMS. The inset in c is a sectional scan of the surface along the direction perpendicular to the waves. d–f), idem, for the reference sample.

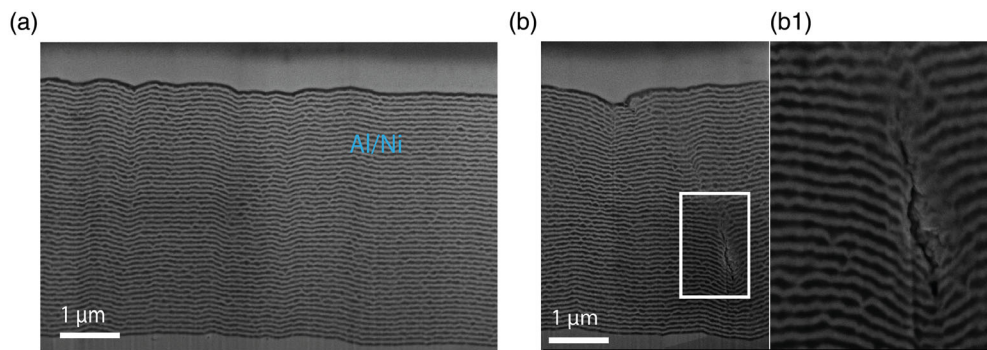


Figure 4. Cross-sectional SEM images of W-RMS deposited on rolled copper: a) structure of the multilayers; b) hole-like defect.

Although it was observed that in self-propagating reactions, the assumption of a constant activation energy is an important tool to quantify the influence of temperature on the reaction rate, it is necessary to point out that this analytical model assumes many parameters of the process to be constants, such as atomic composition, diffusivity, and bilayer thickness.^[7,26,27] The complex morphology of the W-RMS can affect these parameters causing the inaccuracy of the resulting enthalpy. Besides, the temperature was registered in a spot with a diameter of 400 μm in the middle of the sample while the net velocity was calculated in a length of 40 mm. Considering that the W-RMS morphology is not homogeneous and areas with significant defects that could affect the temperature measurement are common, it is possible

that in some cases the temperature is not representative for the average propagation.

3.2.2. Local Propagation

A closer observation of the propagation front (see **Figure 7**) shows that it is affected by the wavy structure of the multilayers. Unlike the radial propagation in the reference samples, the W-RMS presents a propagation front that lengthens in the direction of the waves (x). In the early stage of the propagation, before the reaction reaches the lateral borders of the sample, where the reaction can freely propagate both parallel and perpendicular to the waves, it was observed that the reaction spreads faster parallel

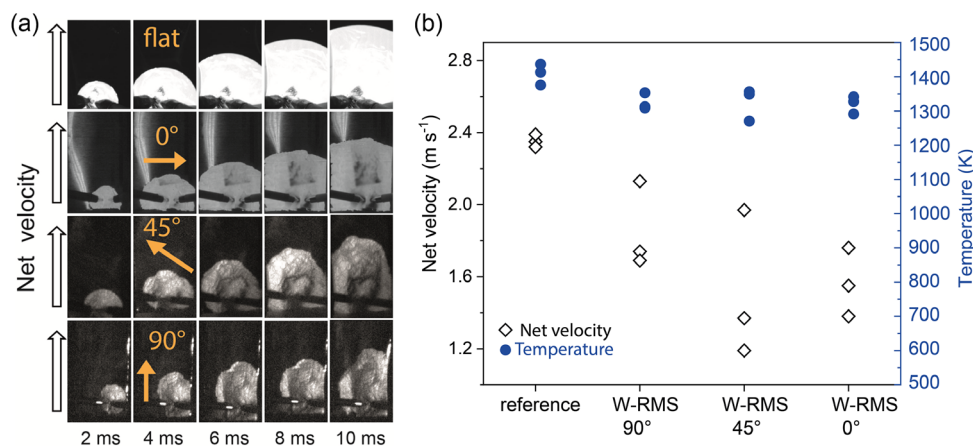


Figure 5. a) Images of the propagation front obtained by the high-speed camera in intervals of 2 ms. The recorded videos can be found in Zenodo (<https://doi.org/10.5281/zenodo.6539366>);^[39] b) plot of the net velocity of values and maximum temperature using the experimental data in listed in Table 1.

Table 1. Net velocity values and maximum temperatures of the propagating flame during the ignition test.

Sample No.	Flat-RMS		W-RMS (90°)		W-RMS (45°)		W-RMS (0°)	
	V [m s ⁻¹]	T _{max} [K]	V [m s ⁻¹]	T _{max} [K]	V [m s ⁻¹]	T _{max} [K]	V [m s ⁻¹]	T _{max} [K]
1	2.4	1350	2.1	1282	1.4	1243	1.4	1264
2	2.3	1412	1.7	1327	1.9	1330	1.6	1301
3	2.4	1338	1.7	1286	1.2	1323	1.8	1315
Mean	2.4	1383	1.8	1298	1.5	1298	1.6	1293
SD	0.05	31.2	0.23	24.9	0.36	48.3	0.21	26.3

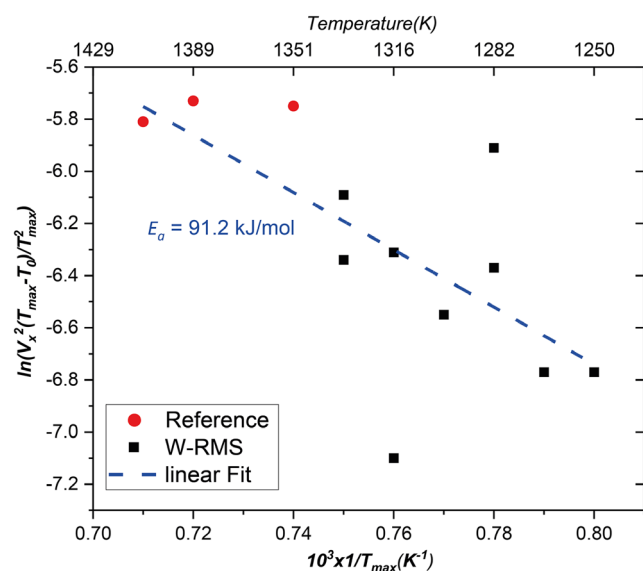


Figure 6. Arrhenius plot generated by replacing data in Table 1 in Equation (1). The dashed line is the linear fit for the points.

to the waves. As shown in Figure 5c depending on the configuration of the sample, 0, 45, or 90, the propagation will be always favored in the direction of the waves.

To determine the velocity of the propagation front in these local areas, we measured the propagation distance from the ignition point to the borders of the front in the directions parallel (x) and normal (y) to the waves 4 ms after the ignition started (see Figure 7). Picturing these two distances as the main axis of an oval, we can clearly see that the propagation is faster in the x direction than in y direction. Nevertheless, during the reaction propagation over the entire area of the sample, it was observed that the propagation front encountered barriers that did not stop the propagation but slowed the propagation velocity in local areas and with different orientations. These barriers are assumed to be surficial or hole-like defects that are not parallel to the waves.

3.3. Characterization After the Self-Propagating Reaction

After the ignition test, the reference sample and the 90° W-RMS were observed by SEM microscopy to analyze the surface of the reacted samples. **Figure 8a** shows the surface of the reference sample after reaction, where the formation of bands normal to the direction of propagation front is evident. These bands or patterns observed in Figure 8a,a1 are traces of an unsteady spin-like propagation that has been observed in previous investigations.^[8,26] These microstructures are the result of fluctuations in the local temperature and in the local rate of the reaction, where some bands reach higher temperatures than others. As

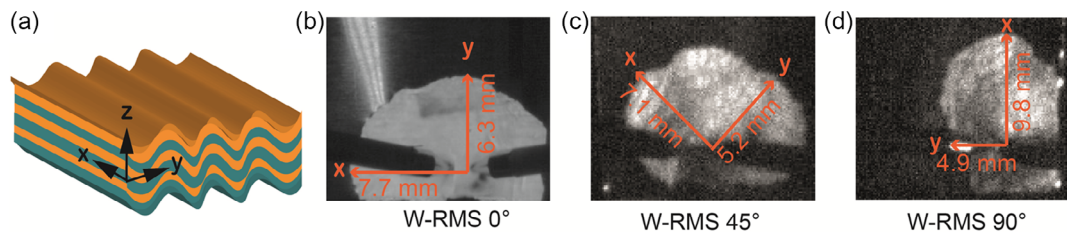


Figure 7. a) 3D scheme of W-RMS pointing directions normal to the layers (z) parallel to the waves (x) and normal to the waves (y); b–d) are captions of the propagation front.

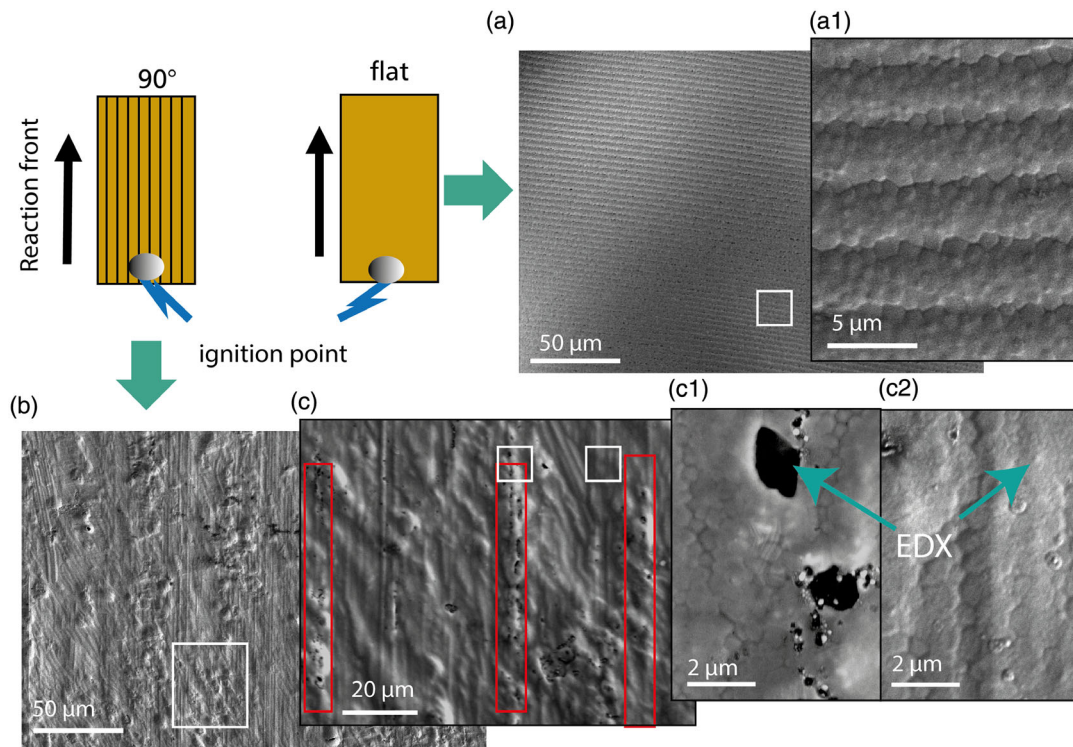


Figure 8. SEM micrographics of the surface of the reactive multilayers after reaction; a,a1) surface views of the reference sample; b,c,c1,c2) surface views of the W-RMS (90°).

a result, the hotter areas present coarse microstructures, whereas the colder areas exhibit fine microstructures.^[2,8,26] In the case of the W-RMS, the bands normal to net reaction front are not observed any more, and the resulting microstructure still retains the orientation of waves that were replicated from the substrate as is observed in Figure 8b,c. A closer view of the surface in Figure 8c1,c2 points some defects (dark spots) in the RMS that are parallel to the orientation of the previous waves. EDX analyses revealed that the areas without defects have an atomic composition of 60 at% Ni and 40 at% Al \pm 2%, whereas the dark spots contain a high percentage of nickel, resulting in 82 at% Ni and 17 at% Al \pm 7%. In the reference samples, the atomic composition in different areas resulted in 60 at% Ni and 40 at% Al with a deviation of 2%.

XRD analysis was performed before and after reaction for the W-RMS and the reference sample produced in a flat Si substrate. It can be observed in Figure 9a that before ignition,

both samples show similar patterns with the reflexes of Al *fcc* (PDF 02-004-0787) and Ni *fcc* (PDF 02-004-0850). After the reaction, both samples present the corresponding reflexes to the B2 phase Al_{0.42}Ni_{0.58} (PDF 02-044-1267); however, the W-RMS presents the reflexes (111) and (200) of the AlNi₃ phase (PDF 02-065-0144) too. These reflexes can be related to the dark spots with excess of Ni that were identified by EDX analysis (Figure 8c1).

4. Discussion

4.1. Impact of the Rough Substrate Surface in the Growth of the W-RMS

Compared to the flat surface of the Si used for the deposition of the reference sample, the copper substrate presents a severely

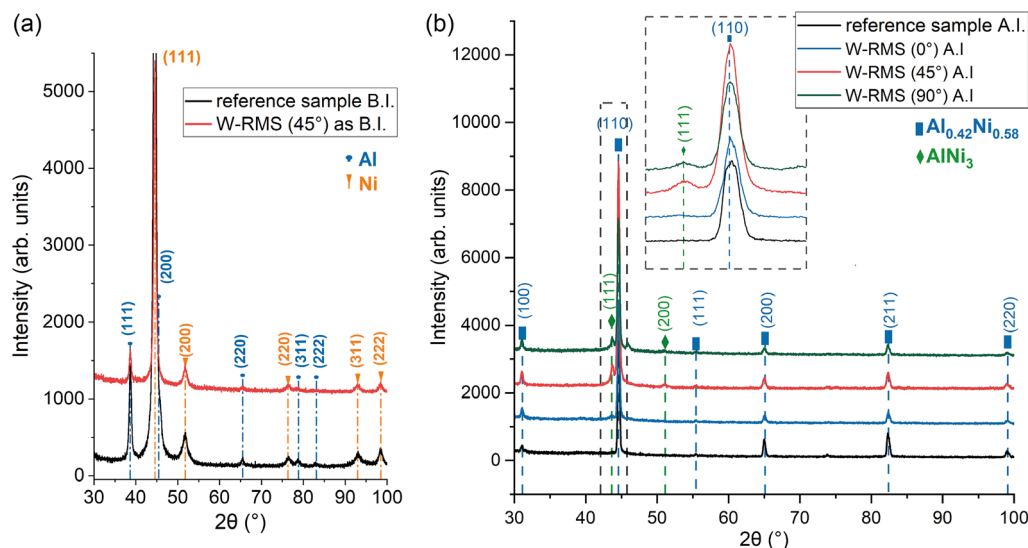


Figure 9. XRD patterns of Al/Ni W-RMS and the reference sample obtained in Bragg–Brentano geometry: a) before ignition; b) after ignition.

rough surface with ridges and grooves that affect the growth of the produced W-RMS, by the effects of shadowing, reemission, and resputtering.^[28,29] As a result, the features of the W-RMS, such as interface roughness, surface topography, and compactness of the reactive foils, are affected giving rise to intermixing areas, local compositional variations, and the formation of growth defects.^[14,18,30] These morphological characteristics of the W-RMS affect the performance of system during the self-propagation. The increase of the intermixing areas in the interface reduces the velocity and the heat of the reaction,^[6] while local compositional variation can produce an oscillating reaction front^[26] and grown defects normal to the layers act as a barrier for the thermal diffusion.^[31]

4.2. Effect of Wavelike Surface Morphology on the Self-Propagation Mechanisms

The propagation front observed during the ignition of the reference sample and the traces of the propagation wave in the shape of bands are characteristic features of RMS.^[8,13,27,32] The formation of bands normal to the direction of the propagation in the reacted foils are evidence of an spinline propagation front.^[8] However, in the W-RMS the propagation front shows an elongated shape (see Figure 7) that indicates that the propagation of the reaction is favored along the direction of the waves. Furthermore, after ignition, the morphology of the resulting microstructures does not present bands normal to the direction of the net propagation but rather retains the surface texture of the W-RMS. These observations evidence that the radial propagation behavior of the reaction was strongly affected by the anisotropic microstructure of the W-RMS. To elucidate the main factors that cause the propagation behavior, the analysis of the self-propagation mechanisms in the W-RMS is needed.

It is well known that the self-propagation in RMS is governed mainly by two mechanisms, the atomic diffusion between the

reactants which occurs normal to the layers (z) and the thermal diffusion which occurs mainly parallel to the layers (x and y). The atomic diffusion will be mainly affected by the atomic composition, thickness of the bilayer, and the intermixing in the interface of the reactants,^[9,33,34] while the thermal diffusion which allows the heat conduction to the unreacted areas depends on thermal conductivity of the materials, the heat capacity, and the density of the RMS.^[1,2,7] Therefore, it is necessary to analyze the impact of the morphology of the RMS on both atomic diffusion and thermal diffusion.

4.3. Influence on the Atomic Diffusion

Under low heating rates, it was observed that roughened interfaces and nodular defects will promote atomic diffusion.^[14,35] This was attributed to the larger contact area between the reactants in the interface, and to the high concentration of vacancies which allows the mobility of the diffusion atoms.^[35,36] This will cause a decrease in the activation energy and will impact in the heat release dynamics, causing that the heat release will be distributed among the reaction stages. Therefore, in the last stages of the reaction, the temperature peaks decrease.^[34,35] For Al/Ni RMS with rough interfaces produced due to the rough substrate surfaces, it was observed that during annealing a roughened interface promotes the atomic diffusion in the interphase resulting in the formation of an intermetallic; this intermetallic phase hinders the atomic diffusion in the flowing stages of the reaction which cause a reduction in the reaction rate.^[14] However, during a self-propagating reaction, which occurs under high heating rates, the atomic diffusion mechanism will change because the reaction occurs in a liquid–solid state, where the formation of the B2 AlNi phase occurs fast and directly.^[16] It can be speculated that these effects will be present in an early stage of the reaction before the aluminum melts, which can decrease the reaction rate and the temperature peaks during self-propagation. This could explain the lower values for temperature and velocity

registered for the W-RMS in comparison with the reference sample. Nevertheless, in order to demonstrate this theory further investigation is necessary.

4.4. Influence on the Thermal Diffusion

The thermal diffusion is directly proportional to the thermal conductivity of the material; in flat RMS, the thermal conductivity is already direction dependent. Normally two main directions are considered, one parallel (x and y) to the layers and other normal (z) to the layers (see Figure 7a).^[27] In the case of the W-RMS due to the presence of waves oriented in a preferential direction, the thermal conductivity will differ in x direction compared with y direction. In y direction, due to the heterogeneous waves, disruptions and hole-like defects are common; these defects decrease the thermal conductivity in this direction.^[37,38] Consequently, the thermal diffusion is favored in the direction of the waves resulting in faster propagation of the reaction in x direction as shown in Figure 5a and 7. Therefore, we presume that the impact of the surficial and bulk defects on the thermal diffusion will be the main responsible for the untypical propagation front.

4.5. Propagation Front and Net Velocity

Considering the anisotropic topography of the W-RMS and the observation of the propagation in local areas of the sample, it is expected that in the samples with the waves oriented at 90° , the net propagation velocity of the front will be faster than in the samples with patterns oriented at 0° and 45° ; however, it is not possible to observe a clearly tendency due to the wide range of variation in our results. As observed in the microstructural investigation of the W-RMS, the transferred patterns were not completely homogeneous and the presence of defects that disturb the waves was also common. The obtained results suggest that these defects influence the propagation in the W-RMS disrupting any preferential propagation along the direction of the waves and causing the variation in the net velocity. On substrates with standard patterns, obtained through a more complex manufacturing process, the influence of an anisotropic surface texture would be stronger.

4.6. Phase Transformation

XRD patterns showed that the reference sample and the W-RMS react, forming AlNi B2 phase. However, in the patterns obtained from W-RMS, two small reflexes are observed that correspond to the AlNi₃ (L3) phase. Furthermore, spots on the surface of the reacted foil, with a composition of around 82 at% Ni, were observed, and the XRD patterns after ignition do not show reflexes of Ni *fcc* or Al *fcc* anymore which indicates that both reactants were consumed. Considering the previous observations, we can presume the presence of the phase L3 in the small spots observed with a high content of Ni. The formation of these two phases was already observed in Al/Ni RMS with an atomic composition rich in nickel.^[10,15] Note that these small spots of the second phase are aligned with the direction of the patterns. To confirm the presence of the L3 phase and elucidate the phase formation process, it is necessary to perform further analyses.

5. Conclusions

Reactive multilayers of Ni/Al with wavelike surface morphology in the shape of free-standing foils were successfully fabricated and the microstructures of the system before and after ignition were analyzed.

The influence of the reproduced waves on the dynamics of the self-propagation front was evidenced. During the reaction, the growth defects in the structure of the W-RMS slow down the velocity of propagation without significantly reducing the maximum temperature. Whereas the net propagation velocity can be reduced by about 50%, the maximum temperature just decreases by about 8% compared to samples prepared on substrates with flat surfaces. This is attributed mainly to hole-like defects and the disruptions in the microstructure caused by the substrate surface topography. The anisotropic microstructure of the produced W-RMS influences not only the propagation velocity but also the propagation front behavior and the resulting microstructure after reaction. However, the effect of surface and bulk defects on phase transformation should be further investigated.

The present study demonstrates the potential to control the propagation behavior of the reaction in RMS by using substrates with rough and oriented surfaces. Moreover, it shows that it is possible to decrease the velocity of propagation and modify the propagation mode without the need to alter the chemical composition of the system during its fabrication.

Acknowledgements

The work was supported by the Deutsche Forschungsgemeinschaft (DFG, grants Scha 632/29 and Scha 632/30 and Scha 632/27 "DFG-Gerätezentrum"). This work was also supported by the free state of Thuringia under grants 2015 FGI 0025 305 (FastXRD) and B715-10009 (BioMacroNano2020), all cofinanced by the European Union within the framework of the European Regional Development Fund (ERDF). Joachim Döll from the Center of Micro- and Nanotechnology (ZMN), a DFG-funded core facility at TU Ilmenau, is gratefully acknowledged for his professional help in the deposition of the samples. The authors would also like to acknowledge the support of Marcus Glaser and Emina Vardo, both from TU Ilmenau, with the ignition experiments.

Open Access funding enabled and organized by Projekt DEAL.

Conflict of Interest

The authors declare no conflict of interest.

Data Availability Statement

The data that support the findings of this study are available from the corresponding author upon reasonable request.

Keywords

Al/Ni multilayers, film morphology, reactive multilayers, self-propagating reactions, surface morphology, velocity of propagation

Received: November 11, 2022
Revised: January 14, 2023
Published online: March 1, 2023

- [1] D. P. Adams, *Thin Solid Films* **2015**, 576, 98.
- [2] T. P. Weihs, *Metallic Films for Electronic, Optical and Magnetic Applications*, Elsevier, Amsterdam, The Netherlands **2014**, pp. 160–243, ISBN 978-0-85709-057-7.
- [3] Y. Ma, D. Bridges, Y. Yu, J. Han, H. Li, A. Hu, *Appl. Sci.* **2019**, 9, 319.
- [4] Y. Zhu, J. Geng, F. Wang, S. Yan, P. Zhao, Q. Meng, J. Wang, Q. Wu, *Z. Anorg. Allg. Chem.* **2020**, 646, 200.
- [5] A. Wang, I. Gallino, S. S. Riegler, Y.-T. Lin, N. A. Isaac, Y. H. Sauni Camposano, S. Matthes, D. Flock, H. O. Jacobs, H.-W. Yen, P. Schaaf, *Mater. Des.* **2021**, 206, 109790.
- [6] A. J. Gavens, D. van Heerden, A. B. Mann, M. E. Reiss, T. P. Weihs, *J. Appl. Phys.* **2000**, 87, 1255.
- [7] M. D. Grapes, T. P. Weihs, *Combust. Flame* **2016**, 172, 105.
- [8] J. P. McDonald, V. C. Hodges, E. D. Jones, D. P. Adams, *Appl. Phys. Lett.* **2009**, 94, 34102.
- [9] R. Knepper, M. R. Snyder, G. Fritz, K. Fisher, O. M. Knio, T. P. Weihs, *J. Appl. Phys.* **2009**, 105, 83504.
- [10] T. S. Dyer, Z. A. Munir, *Metall. Mater. Trans.* **1995**, 26, 603.
- [11] E.-M. Bourim, I.-S. Kang, H. Y. Kim, *Micromachines* **2021**, 12, 1272.
- [12] F. Schwarz, R. Spolenak, *J. Appl. Phys.* **2022**, 131, 75107.
- [13] S. Jayaraman, O. M. Knio, A. B. Mann, T. P. Weihs, *J. Appl. Phys.* **1999**, 86, 800.
- [14] B. Liu, X. Yu, X. Jiang, Y. Qiao, L. You, Y. Wang, F. Ye, *Appl. Surf. Sci.* **2021**, 546, 149098.
- [15] Y. H. Sauni Camposano, S. S. Riegler, K. Jaekel, J. Schmauch, C. Pauly, C. Schäfer, H. Bartsch, F. Mücklich, I. Gallino, P. Schaaf, *Appl. Sci.* **2021**, 11, 9304.
- [16] J. C. Trenkle, L. J. Koerner, M. W. Tate, N. Walker, S. M. Gruner, T. P. Weihs, T. C. Hufnagel, *J. Appl. Phys.* **2010**, 107, 113511.
- [17] (Ed. Schulz, A. E. A.) *Characterization of Reactive Multilayer Systems Deposited on LTCC Featuring Different Surface Morphologies*, MikroSystem Technik Kongress, Stuttgart-Ludwigswurg, **2021**.
- [18] G. M. Fritz, H. Joress, T. P. Weihs, *Combust. Flame* **2011**, 158, 1084.
- [19] S. Danzi, V. Schnabel, X. Zhao, J. Käch, R. Spolenak, *Appl. Phys. Lett.* **2019**, 114, 183102.
- [20] I. Horcas, R. Fernández, J. M. Gómez-Rodríguez, J. Colchero, J. Gómez-Herrero, A. M. Baro, *Rev. Sci. Instrum.* **2007**, 78, 13705.
- [21] C. A. Schneider, W. S. Rasband, K. W. Eliceiri, *Nat. Methods* **2012**, 9, 671.
- [22] Brucker, Diffrac.EVA.
- [23] Digital Surf, *MountainsMap*, **1996**.
- [24] P. Panjan, A. Drnovšek, P. Gselman, M. Čekada, M. Panjan, *Coatings* **2020**, 10, 447.
- [25] R. Armstrong, *Combust. Sci. Technol.* **1990**, 71, 155.
- [26] J. C. Trenkle, J. Wang, T. P. Weihs, T. C. Hufnagel, *Appl. Phys. Lett.* **2005**, 87, 153108.
- [27] L. Alawieh, O. M. Knio, T. P. Weihs, *J. Appl. Phys.* **2011**, 110, 13509.
- [28] T. Karabacak, *J. Nanophotonics* **2011**, 5, 52501.
- [29] M. Salvalaglio, R. Backofen, A. Voigt, *Phys. Rev. B* **2016**, 94, <https://doi.org/10.1103/PhysRevB.94.235432>.
- [30] G. M. Fritz, S. J. Spey, M. D. Grapes, T. P. Weihs, *J. Appl. Phys.* **2013**, 113, 14901.
- [31] H. Bartsch, J. Manuel, R. Grieseler, *Technologies* **2017**, 5, 79.
- [32] D. P. Adams, R. V. Reeves, M. J. Abere, C. Sobczak, C. D. Yarrington, M. A. Rodriguez, P. G. Kotula, *J. Appl. Phys.* **2018**, 124, 95105.
- [33] A. H. Kinsey, K. Slusarski, S. Sosa, T. P. Weihs, *ACS Appl. Mater. Interfaces* **2017**, 9, 22026.
- [34] L. Marín, Y. Gao, M. Vallet, I. Abdallah, B. Warot-Fonrose, C. Tenaillon, A. T. Lucero, J. Kim, A. Esteve, Y. J. Chabal, C. Rossi, *Langmuir* **2017**, 33, 11086.
- [35] B. Julien, J. Cure, L. Salvagnac, C. Josse, A. Esteve, C. Rossi, *ACS Appl. Nano Mater.* **2020**, 3, 2562.
- [36] M. Mursalat, M. Schoenitz, E. L. Dreizin, *Fuel* **2022**, 324, 124538.
- [37] R. L. Xu, M. Muñoz Rojo, S. M. Islam, A. Sood, B. Vareskic, A. Katre, N. Mingo, K. E. Goodson, H. G. Xing, D. Jena, E. Pop, *Journal of Applied Physics* **2019**, 126, 185105.
- [38] Y. Yan, S. C. King, M. Li, T. Galy, M. Marszewski, J. S. Kang, L. Pilon, Y. Hu, S. H. Tolbert, *J. Phys. Chem. C* **2019**, 123, 21721.
- [39] Y. H. Sauni Camposano, Self-propagation of reactive Al/Ni multilayers with textured surface topography, **2022**, <https://doi.org/10.5281/zenodo.6539366>.